Soft Matter

COMMUNICATION

Magneto-induced stress enhancing effect in a colloidal suspension of paramagnetic and superparamagnetic particles dispersed in a ferrofluid medium†

Cite this: *Soft Matter*, 2014, **10**, 813

Received 13th November 2013
Accepted 27th November 2013

DOI: 10.1039/c3sm52865k

www.rsc.org/softmatter

Taixiang Liu, Xinglong Gong,* Yangguang Xu and Shouhu Xuan*

The magneto-induced stress and relative microstructure in a colloidal suspension of paramagnetic and superparamagnetic particles dispersed in a ferrofluid medium is studied using particle-level dynamics simulation. It shows that the stress perpendicular to the direction of an external uniaxial magnetic field can be strongly enhanced by increasing the ratio of paramagnetic particles to approaching that of superparamagnetic particles. The magnetic field-induced net-like or embedded chain-like microstructures formed by paramagnetic and superparamagnetic particles contribute to this stress enhancing effect.

The colloidal suspension of paramagnetic and superparamagnetic particles (SPSP) in a ferrofluid medium is a novel smart magneto-controllable particulate composite,[1] which is usually prepared by dispersing micro-sized paramagnetic (or diamagnetic) and superparamagnetic particles into a ferrofluid matrix. As the physical or mechanical properties of this suspension can be controlled by an external magnetic field, more and more researchers are devoted to studying the mechanism and to exploiting the applications of this suspension. The sketch of the colloidal suspension is illustrated in Fig. 1. In the suspension, the permeability of the ferrofluid matrix can be tuned by adjusting the concentration of internal nano-sized magnetic particles. The permeability of dispersed micro-sized paramagnetic particles is usually smaller than that of the ferrofluid matrix, while the permeability of dispersed micro-sized superparamagnetic particles is larger than that of the ferrofluid matrix. So in the presence of an external magnetic field, the paramagnetic particle will be magnetized and obtain an anti-parallel magnetic moment to the external magnetic field, behaving as a diamagnetic particle. Given this and corresponding to Byrom and Biswal's work,[1] in the following content of this communication, we denote the paramagnetic particles as "diamagnetic" particles and no longer distinguish whether the particles are paramagnetic or diamagnetic under the usual conditions. Here, we use a characterization of the particle relative to the ferrofluid matrix. The superparamagnetic particles will be magnetized parallel to the external magnetic field and we denote the particles as "paramagnetic" particles in the suspension.

For magneto-controllable colloidal suspensions, it is widely recognized that their macroscopic physical and/or mechanical properties directly depend on their interior microstructures. Generally, chain-like or column-like microstructures will form when the homogeneous magnetic or magnetized particle colloidal suspension is subjected to an external uniaxial magnetic field.[2,3] These microstructures are simple and they reduce the variety of structures that can be formed. This limits the applicability of the suspension to study other phenomena, such as magneto-gelation,[4] magneto-seals,[5] and magneto-valves.[6,7] To increase the

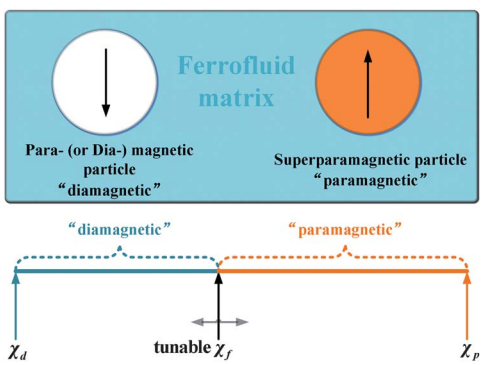

Fig. 1 The sketch of the colloidal suspension of paramagnetic (or diamagnetic) and superparamagnetic particles. χ_d, χ_f, and χ_p are the susceptibilities of paramagnetic (or diamagnetic) particles, ferrofluid matrix, and superparamagnetic particles, respectively, and have the magnitude relationship of $\chi_d < \chi_f < \chi_p$ in the presence of an external vertical magnetic field.

CAS Key Laboratory of Mechanical Behavior and Design of Materials, Department of Modern Mechanics & Collaborative Innovation Center of Suzhou Nano Science and Technology, University of Science and Technology of China, Hefei, Anhui, 230027, China. E-mail: gongxl@ustc.edu.cn; xuansh@ustc.edu.cn; Fax: +86 551 63600419; Tel: +86 551 63600419

† Electronic supplementary information (ESI) available. See DOI: 10.1039/c3sm52865k

diversity of magneto-induced structures and to study the structure-based properties, one way is to configure a diverse non-uniform external magnetic field. But this way is usually too complex or difficult to get or control an anticipatory structure in experiment. Another way is to mix various particles with different magnetic properties and/or sizes. Sedlacik *et al.*[8–10] studied the synthesis and characterization of different kinds of particles. From an experimental study, Ulicny *et al.*[11] found an enhancement in the magnetic field-induced yield stress of magnetorheological fluids caused by the presence of non-magnetizable particles. Recently, an experimental study on the colloidal system of paramagnetic particles (Dynabeads® M-270 streptavidin, produced by Invitrogen, Grand Island, NY) and diamagnetic particles (melamine resin beads, provided by Sigma-Aldrich, St. Louis, MO) in a ferrofluid medium (fluidMAG-PAS, produced by Chemicell-GmbH, Berlin) was carried out by Byrom and Biswal,[1] observing two-dimensional fractal aggregates which grew in both the directions parallel and perpendicular to the external magnetic field. Liang *et al.*[12] presented an enhanced separation experiment of magnetic and diamagnetic particles in a dilute ferrofluid, demonstrating that altering the susceptibility of the matrix can significantly change the properties of the colloidal suspension of magnetic and diamagnetic particles. Besides, colloidal suspensions of dielectric particles with oppositely oriented induced dipole moments were studied by Gangwal *et al.*[13] and Schmidle *et al.*,[14] demonstrating that unusual two-dimensional colloidal networks will form under a high frequency alternating current (AC) electric field. Furthermore, magnetic self-assembly was found to be capable of organizing a diverse set of colloidal particles into highly reproducible, rotationally symmetric arrangements.[15–18] The aforementioned studies bring us inspiring experimental results, as well as some relative qualitative explanations.

However, as is pointed out by Faraudo *et al.*,[19] it is clear that theoretical concepts and methods progress at a slow pace compared to the impressive development of experiments. We lack a full understanding of the formation mechanism of the particulate microstructure in the suspensions of different kinds of particles with different magnetic properties and/or sizes, and the microstructure-based macroscopic physical or mechanical properties. In this communication, particle-level dynamics simulation is employed to analyse the magneto-induced stress state and stress-relevant microstructure of the SPSP with different particle concentrations and different ratios of diamagnetic particles to paramagnetic particles. The key point of this work is to study how the ratio of diamagnetic particles to paramagnetic particles dispersed in the ferrofluid matrix affects the magneto-induced microstructure and the microstructure-based macroscopic properties of the SPSP.

For the colloidal suspension of paramagnetic particles in a ferrofluid, the susceptibility of the ferrofluid can be easily tuned by adjusting the volume fraction of magnetic nanoparticles in the deionized water solution:[1]

$$\chi_f = \frac{\mu_0 {M_s}^2 \phi_m V}{3 k_B T}. \quad (1)$$

In the expression, μ_0 is the permeability of vacuum, M_s is the saturation magnetization of the magnetic nanoparticles, ϕ_m is the volume fraction of magnetic nanoparticles in the ferrofluid, V is the volume of a single magnetic nanoparticle, k_B is the Boltzmann constant, and T is the colloidal absolute temperature. When placing a micro-sized paramagnetic particle into the ferrofluid and applying an external magnetic field to the system, the particle will acquire a dipole magnetic moment:

$$\boldsymbol{m} = V\boldsymbol{M} = \frac{4\pi a^3}{3} 3K\boldsymbol{H} = 4\pi a^3 K\boldsymbol{H}. \quad (2)$$

$$K = \frac{\chi_p - \chi_f}{\chi_p + 2\chi_f + 3}$$

where a is the radius of the particle, K is the Clausius–Mossotti factor relating the magnetic susceptibility of the particle to that of the ferrofluid, χ_p is the susceptibility of the particle, and $\boldsymbol{H}$ is the applied external magnetic field. Here, as the placed micro-sized particle is two orders of magnitudes larger than the magnetic nanoparticle in dilute ferrofluid (ϕ_m < 5.0%), to simplify the modelling and analysis, the ferrofluid is considered as a continuum medium either in the presence of or in the absence of an external magnetic field. Eqn (2) shows, as well as Fig. 1 illustrates, that the particle can exhibit a dipole either parallel (paramagnetic) or antiparallel (diamagnetic) to the external magnetic field, depending on its susceptibility being either larger or smaller than that of the ferrofluid. Increasing the ferrofluid concentration has an effect of increasing the moment of the diamagnetic dipole and decreasing the moment of the paramagnetic dipole simultaneously. After the dispersed particles acquire paramagnetic or diamagnetic dipole moments under an external magnetic field, they will form some certain magneto-induced aggregates through particle–particle and particle–matrix interactions.

When a particle, marked as particle i, is magnetized as a dipole, it will produce an induced magnetic field in its surroundings:

$$\boldsymbol{H}_i = -\frac{\boldsymbol{m}_i}{4\pi r^3} + \frac{3(\boldsymbol{m}_i \cdot \boldsymbol{r})\boldsymbol{r}}{4\pi r^5} \quad (3)$$

where $\boldsymbol{m}_i$ is the magnetic dipole moment of particle i, $\boldsymbol{r}$ is the spatial vector from particle i to a spatial field point and r is the norm of $\boldsymbol{r}$. The other magnetized particle j will induce a magnetic field applied on particle i as:

$$\boldsymbol{H}_{ij} = -\frac{\boldsymbol{m}_j}{4\pi {r_{ij}}^3} + \frac{3(\boldsymbol{m}_j \cdot \boldsymbol{r}_{ij})\boldsymbol{r}_{ij}}{4\pi {r_{ij}}^5}, \quad (4)$$

in which $\boldsymbol{m}_j$ is the magnetic dipole moment of particle j, $\boldsymbol{r}_{ij}$ is the positional vector from particle j to particle i and r_{ij} is the norm of $\boldsymbol{r}_{ij}$. Then the magnetic dipole moment of particle i will be updated as:

$$\boldsymbol{m}_i = 4\pi {a_i}^3 K\left(\boldsymbol{H} + \sum_{j=1, j\neq i}^{N} \boldsymbol{H}_{ij}\right), \quad (5)$$

in which N is the total number of the particles in the considered system. With the magnetized particle i and particle j, the

interparticle magnetic force between them can be described using the classical dipole approximation:

$$\boldsymbol{F}_{ij}^{\mathrm{m}} = \frac{3\mu_0}{4\pi {r_{ij}}^5}\left(m_{ij} - 5m_{ir}m_{jr}\right)\boldsymbol{r}_{ij} + \frac{3\mu_0}{4\pi {r_{ij}}^4}\left(m_{jr}\boldsymbol{m}_i + m_{ir}\boldsymbol{m}_j\right), \quad (6)$$

with $m_{ij} = \boldsymbol{m}_i \cdot \boldsymbol{m}_j$, $m_{ir} = \boldsymbol{m}_i \cdot \boldsymbol{r}_{ij}/r_{ij}$, and $m_{jr} = \boldsymbol{m}_j \cdot \boldsymbol{r}_{ij}/r_{ij}$. Hereto, the magnetic interaction between magnetized particles is modelled on matter whether the particle is paramagnetic or diamagnetic. The ground states of magnetic interactions among paramagnetic and/or diamagnetic particles under an external magnetic field are illustrated in Fig. 2.

The interparticle van der Waals force is also taken into account when modelling the particle–particle interaction. This force can be expressed as:[20]

$$\boldsymbol{F}_{ij}^{\mathrm{vdw}} = \frac{16A}{\left(L_{\mathrm{r}}+2\right)^3\left({L_{\mathrm{r}}}^2+4L_{\mathrm{r}}\right)^2}\frac{\boldsymbol{r}_{ij}}{r_{ij}} \quad (7)$$

where A is the Hamaker constant, and $L_r = 2(r_{ij} - d_{ij})/d_{ij}$ and $d_{ij} = (a_i + a_j)$. a_i and a_j are the radius of the particle i and particle j, respectively. To avoid the interparticle overlap, the excluded-volume force is introduced as:[21]

$$\boldsymbol{F}_{ij}^{\mathrm{ev}} = \frac{3\mu_0 m_{ij}}{2\pi {r_{ij}}^5}\exp\left[-10\left(r_{ij}/d_{ij}-1\right)\right]\cdot\boldsymbol{r}_{ij}. \quad (8)$$

The force can balance the interparticle magnetic force when the particles are in contact with each other.

When the particle i moves in the ferrofluid matrix with a low Reynolds number, the hydrodynamics drag force applied on it can be characterized by the Stokes force as:

$$\boldsymbol{F}_i^{\mathrm{h}} = -\xi_{\mathrm{t}}\cdot\boldsymbol{U}. \quad (9)$$

Here, $\xi_{\mathrm{t}} = 6\pi\eta_{\mathrm{f}}a_i$ is the translational drag coefficient, $\boldsymbol{U}$ is the moving velocity of the particle relative to its surrounding ferrofluid matrix. η_{f} is the viscosity of the ferrofluid matrix and a_i is the radius of the particle i. Besides, the stochastic Brownian force $\boldsymbol{F}_i^{\mathrm{B}}$ applied on particle i arising from the thermal fluctuations in the ferrofluid can be characterized by:[22]

$$\langle\boldsymbol{F}_i^{\mathrm{B}}\rangle = 0 \text{ and } \langle\boldsymbol{F}_i^{\mathrm{B}}(0)\boldsymbol{F}_i^{\mathrm{B}}(t)\rangle = 2k_{\mathrm{B}}T\mathbf{R}_{\mathrm{FU}}\delta(t) \quad (10)$$

where $\mathbf{R}_{\mathrm{FU}}$ is the configuration-dependent resistance matrix that gives the hydrodynamic force on the particles due to its motion relative to the fluid, and $\delta(t)$ is the Dirac-delta function. To the translational motion of particle i, the resistance matrix can be simplified to a resistance coefficient ξ_{t}. The resultant force of gravity and buoyancy applied on particle i is:

$$\boldsymbol{F}_i^{\mathrm{gb}} = \frac{4\pi {a_i}^3}{3}\left(\rho_{\mathrm{p}} - \rho_{\mathrm{f}}\right)\boldsymbol{g} \quad (11)$$

in which, ρ_{p} and ρ_{f} are the densities of particle and ferrofluid, respectively. $\boldsymbol{g}$ is the gravitational acceleration. The values of main physical parameters in the computation are based on what they are in the experiment of Byrom and Biswal[1] and are listed in Table 1.

With the aforementioned forces, the motion of particle i can be governed by the kinematic equation:

$$\frac{4\pi {a_i}^3\rho_{\mathrm{p}}}{3}\cdot\frac{\mathrm{d}^2\boldsymbol{r}}{\mathrm{d}^2t} = \sum_{j\neq i}\left(\boldsymbol{F}_{ij}^{\mathrm{m}} + \boldsymbol{F}_{ij}^{\mathrm{vdw}} + \boldsymbol{F}_{ij}^{\mathrm{ev}}\right) + \boldsymbol{F}_i^{\mathrm{h}} + \boldsymbol{F}_i^{\mathrm{B}} + \boldsymbol{F}_i^{\mathrm{gb}} \quad (12)$$

where $\boldsymbol{r}$ is the position vector of particle i. As the particle is paramagnetic or diamagnetic, the magnetic torque applied on the particle is so small that the magneto-induced rotational motion of the particle can be neglected. In eqn (12), $|\boldsymbol{F}_i^{\mathrm{gb}}| = O(10^{-7})$ μN is constant to particle i. $\langle\boldsymbol{F}_i^{\mathrm{B}}\rangle \sim \sqrt{\langle\boldsymbol{F}_i^{\mathrm{B}}(0)\boldsymbol{F}_i^{\mathrm{B}}(t)\rangle} = \sqrt{2k_{\mathrm{B}}T\mathbf{R}_{\mathrm{FU}}\delta(t)} = O(10^{-7})$ μN. $|\boldsymbol{F}_i^{\mathrm{h}}| = 0 \sim O(10^{-7})$ μN, which is relevant to the velocity of particle i. To estimate the interparticle forces $\boldsymbol{F}_{ij}^{\mathrm{m}}$, $\boldsymbol{F}_{ij}^{\mathrm{vdw}}$ and $\boldsymbol{F}_{ij}^{\mathrm{ev}}$, the situation of two contact particles with equal diameter of 1.5 μm and the orientations of the magnetic moments parallel to the positional vector is discussed. Then we can have $|\boldsymbol{F}_{ij}^{\mathrm{m}}| = 3\mu_0 {m_i}^2/(32\pi {a_i}^4) = O(10^{-5})$ μN, $|\boldsymbol{F}_{ij}^{\mathrm{vdw}}| = \frac{A}{24}\frac{d_{ij}}{{h_{\min}}^2} = O(10^{-8})$ μN, and $|\boldsymbol{F}_{ij}^{\mathrm{ev}}| = O(10^{-5})$ μN. It can be seen that the interparticle magnetic force $\boldsymbol{F}_{ij}^{\mathrm{m}}$ and excluded-volume force $\boldsymbol{F}_{ij}^{\mathrm{ev}}$ are the dominant forces in the colloidal suspension in the presence of an external magnetic field. In the absence of an external magnetic field, $\boldsymbol{F}_i^{\mathrm{B}}$, $\boldsymbol{F}_i^{\mathrm{gb}}$ and $\boldsymbol{F}_{ij}^{\mathrm{vdw}}$ will drive particles to move, while $\boldsymbol{F}_i^{\mathrm{h}}$ will hinder the particle motion. The numerical solution of eqn (12) can be obtained using the velocity-Verlet integral scheme.[23]

In the simulation, a cubic cell with edge length 50 μm and a quadrate cell with edge length 150 μm are considered for three-dimensional and two-dimensional cases, respectively. Periodic boundary conditions are applied to all sides for the two cases. The integral time step is set as 5.0 μs and the number of total time steps is 1.0×10^5. When the colloidal suspension gets a quasi-stable state under an external magnetic field, the internal forces will achieve a self-balancing state, and the interparticle magnetic force behaves as the governing active force. Therefore, to quantitatively characterize the state of the magneto-induced particulate aggregates, we introduce the microstructure-based magneto-induced stress tensor:

$$\boldsymbol{\sigma} = \frac{1}{V}\sum_{i=1}^{N-1}\sum_{j=i+1}^{N}\boldsymbol{r}_{ij}\boldsymbol{F}_{ij}^{\mathrm{m}}. \quad (13)$$

Here, V is the volume of the considered cubic cell. N is the total number of particles. $\boldsymbol{r}_{ij}$ is the relative positional vector from particle i to particle j. $\boldsymbol{F}_{ij}^{\mathrm{m}}$ is the interparticle magnetic force of particle i and particle j. The axial stress along the direction of an

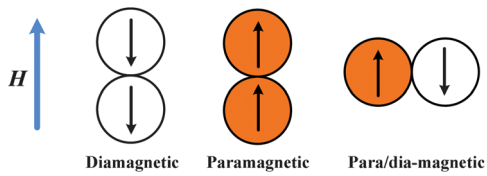

Fig. 2 The ground states of magnetic interactions among paramagnetic and/or diamagnetic particles. Paramagnetic (or diamagnetic) particles will approach each other with head to tail arrangement along the direction of an external magnetic field, while paramagnetic and diamagnetic particles will approach with side by side arrangement perpendicular to the external magnetic field.

Table 1 The values of main parameters in the computation (ref. 1)[a]

Parameter	Physical meaning	Value
ρ_p	Density of paramagnetic particles	1.60 g cm^{-3}
	Density of diamagnetic particles	1.51 g cm^{-3}
a	Average radius of paramagnetic particles	1.4 μm
	Average radius of diamagnetic particles	1.5 μm
χ_p	Susceptibility of paramagnetic particles	0.96
	Susceptibility of diamagnetic particles	0.00
χ_f	Susceptibility of the ferrofluid	0.00–0.96
ρ_f	Density of the ferrofluid	1.00 g cm^{-3}
η_f	Viscosity of the ferrofluid	0.01 Pa s
$\|\boldsymbol{H}\|$	Magnetic strength	11.2 kA m^{-1}
$\|\boldsymbol{g}\|$	Gravitational acceleration	9.80 m s^{-2}
T	Colloidal absolute temperature	298.0 K
A	Hamaker constant	5.0×10^{-19} J
μ_0	Permeability of vacuum	1.27×10^{-6} N A^{-2}
k_B	Boltzmann constant	1.38×10^{-23} N m K^{-1}

[a] 'N' in the 'Value' column is the unit of force: kg m s^{-2}.

external magnetic field is denoted as σ_z and the other two orthogonal axial stresses are denoted as σ_x and σ_y, respectively. The strength of axial stresses perpendicular to the direction of the external magnetic field is taken as $(\sigma_x + \sigma_y)/2$, which is the mean value of max and min stress strength:

$$\left.\begin{matrix}\sigma_{max}\\ \sigma_{min}\end{matrix}\right\} = \frac{\sigma_x + \sigma_y}{2} \pm \sqrt{\left(\frac{\sigma_x - \sigma_y}{2}\right)^2 + {\tau_{xy}}^2} \quad (14)$$

in which, τ_{xy} is the strength of the shear stress between x and y axes.

To the SPSP, the volume fraction of total particles (paramagnetic and diamagnetic particles) is denoted as φ, the ratio of diamagnetic particles to total particles is denoted as λ (that is the ratio of diamagnetic to paramagnetic particles is $\lambda : (1 - \lambda)$), and the ratio of the magnitude of the magnetization of diamagnetic particles M_d to that of paramagnetic particles M_p is denoted as γ (namely, $\gamma = M_d/M_p$). The alteration of other parameters (such as the susceptibility of ferrofluid χ_f, the quantity of particles, and the external magnetic strength H) finally results in the change of the magnitude of paramagnetic dipole moment M_p and the values of the three parameters: φ, λ, and γ. The size distribution of the paramagnetic and diamagnetic particles can be characterized using a log-normal distribution density function:

$$P(d) = \frac{1}{d\sigma\sqrt{2\pi}} \exp\left[-\frac{(\ln(d) - \mu)^2}{2\sigma^2}\right] \quad (15)$$

where d is the diameter of particle, μ and σ are the expectation and standard deviation of $\ln(d)$, respectively. In the computation, $\mu = 1.03$ and 1.10 for the paramagnetic and diamagnetic particles, respectively. $\sigma = 0.30$ for both the particles.

The magneto-induced stress states of SPSP with different ratios of diamagnetic particles are presented in Fig. 3. Firstly, it can be found that all the stress–ratio curves are symmetrical at $\lambda = 0.50$ on the whole. This is because $\gamma = 1.0$, that is the paramagnetic and diamagnetic particles have the same magnitude of magnetization but with opposite orientations. In other words, for example, the particulate system of $\lambda = 0.20$ is equivalent in mechanics to the particulate system of $\lambda = 0.80$, and $\lambda = 0.20$ will transfer to be $\lambda = 0.80$ if we oppositely change the orientations of both the paramagnetic and diamagnetic particles in the system of $\lambda = 0.20$. The subsequent discussions of the stress states will only concern the particulate systems from $\lambda = 0.00$ to $\lambda = 0.50$. The axial stresses σ_z along the direction of an external magnetic field with different φ and λ are shown in the left subfigure of Fig. 3. When the volume fraction of total particles is small, $\varphi = 5.0\%$ for an example, σ_z will decrease slightly with the increase of λ, and the drop of σ_z is 29.2% from $\lambda = 0.00$ to 0.50. The same trend occurs in the systems of $\varphi = 10.0\%$, but the drop of σ_z is 7.3%. For the condition of $\varphi = 12.5\%$, the fluctuation of stress σ_z is less than 5.0%. When φ reaches 15.0%, σ_z shows a magneto-induced enhancing effect with the increase of λ on the whole, and the enhancement of σ_z is 14.2% though a small drop also exists in the case of $\lambda < 0.05$. When φ increases to 20.0%, σ_z shows a magneto-induced enhancing effect with the increase of λ and the enhancement of σ_z reaches 31.2%. Compared to σ_z, the

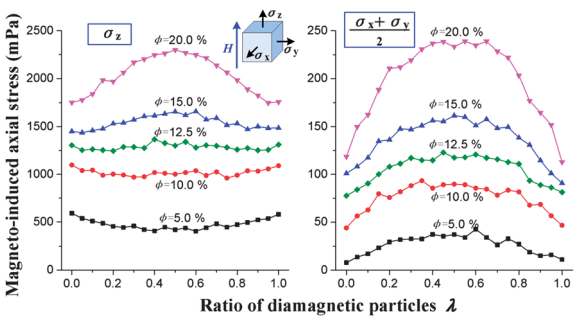

Fig. 3 The magneto-induced axial stress of particulate systems with different volume fractions φ and ratios of diamagnetic particles λ. The left subfigure shows the stress σ_z along the direction of an external magnetic field. The right subfigure shows the mean value of the two orthogonal axial stresses σ_x and σ_y (both perpendicular to the direction of the external magnetic field).

transverse stress $(\sigma_x + \sigma_y)/2$ shows a strong magneto-induced enhancing effect for all φ values with the increase of λ. The enhancements reach 365.6%, 104.5%, 58.3%, 107.1% and 96.9% for $\varphi = 5.0\%$, 10.0%, 12.5%, 15.0% and 20.0%, respectively, from $\lambda = 0.00$ to $\lambda = 0.50$. It is worth noting that both the axial stress along the direction of an external magnetic field and the transverse stress perpendicular to the field direction are strongly enhanced with the increase of the ratio of diamagnetic particles for the volume fraction of total particles being larger than 12.5%.

To understand the microstructure-based mechanism of the magneto-induced stress enhancing effect, the microstructure in a two-dimensional (2D) case is studied firstly. The 2D case is actually a special three-dimensional (3D) case with all the particles being coplanar. The external magnetic field H is set as 11.2 kA m^{-1}. φ is set as 20.0%. γ is set as 1.0. The magneto-induced microstructures with $\lambda = 0.00$ and $\lambda = 0.50$ are illustrated in Fig. 4, in which the edge length is 150.0 μm. The left subfigures of Fig. 4 show the initial random dispersion of particles in the colloidal suspensions and the right subfigures show the relative final microstructures after applying a steady uniaxial external magnetic field. For the condition of $\lambda = 0.00$, namely there are no diamagnetic particles in the colloidal suspension, the paramagnetic particles in the suspension will form chain-like microstructures along the direction of an external magnetic field. For the condition of $\lambda = 0.50$, the number of diamagnetic particles in the suspension is the same as that of the paramagnetic particles, the aggregates of all the particles will grow in both the directions parallel and perpendicular to the external magnetic field. The perpendicular growth of the particle aggregates results from the interaction of paramagnetic and diamagnetic particles (as the ground state of "para/dia-magnetic" shown in Fig. 2). This is an interesting phenomenon that the SPSP will swell not only in the direction of the uniaxial external magnetic field but also in the direction perpendicular to the field (more illustrations can be found in the ESI†).

The 3D magneto-induced microstructures of the colloidal suspension with different ratios of the diamagnetic particles are illustrated in Fig. 5, in which the edge length of the considered cubic cell is 50 μm. When $\lambda = 0.00$, the particles will form column-like structures along the direction of an external magnetic field. These structures formed by paramagnetic particles are similar to the structures formed by soft magnetic particulate composite in our previous studies.[24,25] For the condition of $\lambda = 0.10$, namely there is a small number of diamagnetic particles in the total particles, the main microstructures are also the column-like structures formed by paramagnetic particles. Simultaneously, the diamagnetic particles adhere to the column-like structures. The diamagnetic particles are mainly separate from each other and fill the space among the column-like structures formed by paramagnetic particles. When λ increases to 0.25, the diamagnetic particles will form some short chain-like structures filling the space among the chain-like or column-like structures formed by paramagnetic particles. The diamagnetic particles are no longer separate from each other and form chains contributing to the whole structure. Increasing λ to 0.50, as shown in the bottom-right subfigure of Fig. 5, the diamagnetic and paramagnetic particles play a coequal role contributing to the whole microstructure. The particles aggregate to form chain-like or column-like structures with other particles having the same magnetic properties. The diamagnetic particle chains blend with the paramagnetic chains and both kinds of the chains adhere to each other side by side (as shown in the central inset of Fig. 5). This results in the dispersal uniformity of all the particles and the

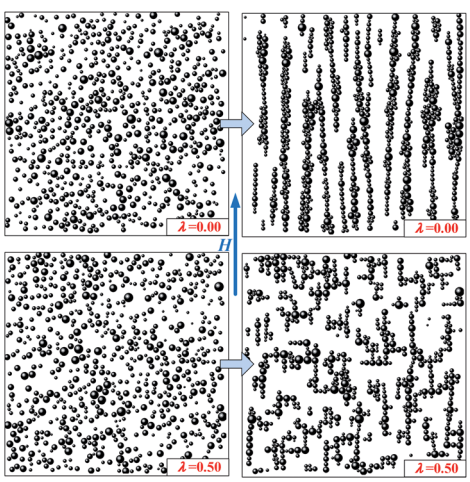

Fig. 4 The magneto-induced 2D microstructures with ($\varphi = 20.0\%$, λ, $\gamma = 1.0$) and $H = 11.2$ kA m^{-1}. The left subfigures show the initial random dispersion of particles in the colloidal suspensions with $\lambda = 0.00$ and 0.50, respectively. The right subfigures show the final microstructure relative to their origins after applying a steady uniaxial external magnetic field.

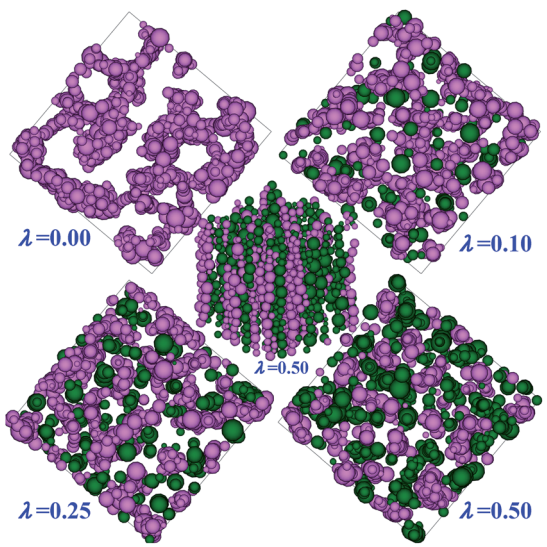

Fig. 5 The magneto-induced 3D microstructures with ($\varphi = 20.0\%$, λ, $\gamma = 1.0$) and $H = 11.2$ kA m^{-1}. All the subfigures show the final magneto-induced microstructures with relative λ. The central inset is the axonometric view of $\lambda = 0.50$ and the others are the top views of $\lambda = 0.00$, 0.10, 0.25, and 0.50, respectively. The lilac balls denote the paramagnetic particles and the dark green balls denote the diamagnetic particles.

magneto-induced stress in both the directions of longitudinal and transverse to the external steady uniaxial magnetic field.

The magneto-induced stress enhancing effect results from the fact that both the paramagnetic and diamagnetic particles can form chain-like structures, and the paramagnetic and diamagnetic chains attract each other side by side (as shown in the central subfigure of Fig. 5). An enhanced magneto-rheological effect using non-magnetizable particles was reported by Klingenberg *et al.*[26,27] and they explained the effect in part to be resulting from the fact that the non-magnetizable particles enhance the non-magnetic repulsive force of magnetizable particles. Here, for the SPSP, we demonstrate that the magneto-induced enhancing effect results from the magnetic interaction between the paramagnetic and diamagnetic particles.

In conclusion, the magneto-induced stress and stress-relevant microstructure of the SPSP was studied using particle-level dynamics simulation. It shows that the magneto-induced transverse stress (perpendicular to the direction of an external magnetic field) can be greatly enhanced by increasing the ratio of diamagnetic particles to approaching that of paramagnetic particles. The simulation reveals that the magneto-induced transverse stretched net-like structures or embedded chain-like structures formed by paramagnetic particles and diamagnetic particles contribute to the transverse stress enhancing effect. When the magnitude of the diamagnetic dipole moment is equal to that of the paramagnetic dipole moment and the volume fraction of total particles is larger than 12.5 v/v%, increasing the ratio of diamagnetic particles will also enhance the axial stress strength along the direction of an external magnetic field, while there is a small reduction in this stress when the volume fraction is below 12.5 v/v%. The enhancing effect of the axial stress results from the fact that both the paramagnetic and diamagnetic particles can form chain-like structures, as well as the paramagnetic chains and diamagnetic chains tightly attracting each other side by side.

Acknowledgements

Financial support from the National Natural Science Foundation of China (Grant no. 11072234, 11125210, 11102202) and the National Basic Research Program of China (973 Program, Grant no. 2012CB937500) is gratefully acknowledged.

Notes and references

1 J. Byrom and S. L. Biswal, *Soft Matter*, 2013, **9**, 9167.
2 G. Bossis, P. Lancon, A. Meunier, L. Iskakova, V. Kostenko and A. Zubarev, *Phys. A*, 2013, **392**, 1567.
3 T. X. Liu, R. Gu, X. L. Gong, S. H. Xuan, H. A. Wu and Z. Zhang, *Magnetohydrodynamics*, 2010, **46**, 257.
4 M. Furlan, B. Brand and M. Lattuada, *Soft Matter*, 2010, **6**, 5636.
5 T. Borbáth, D. Bica, I. Potencz, L. Vékás, I. Borbáth and T. Boros, *IOP Conf. Ser.: Earth Environ. Sci.*, 2010, **12**, 012105.
6 W. H. Li, H. Du and N. Q. Guo, *Int. J. Adv. Manuf. Technol.*, 2003, **21**, 438.
7 M. Y. Salloom and Z. Samad, *Int. J. Adv. Manuf. Technol.*, 2012, **58**, 279.
8 M. Sedlacik, R. Moucka, Z. Kozakova, N. E. Kazantseva, V. Pavlinek, I. Kuritka, O. Kaman and P. Peer, *J. Magn. Magn. Mater.*, 2013, **326**, 7.
9 M. Sedlacik, V. Pavlinek, P. Saha, P. Svrcinova and P. Filip, *Mod. Phys. Lett. B*, 2012, **26**, 1150013.
10 M. Sedlacik, V. Pavlinek, R. Vyroubal, P. Peer and P. Filip, *Smart Mater. Struct.*, 2013, **22**, 035011.
11 J. C. Ulicny, K. S. Snavely, M. A. Golden and D. J. Klingenberg, *Appl. Phys. Lett.*, 2010, **96**, 231903.
12 L. T. Liang, C. Zhang and X. C. Xuan, *Appl. Phys. Lett.*, 2013, **102**, 234101.
13 S. Gangwal, A. Pawar, I. Kretzschmar and O. D. Velev, *Soft Matter*, 2010, **6**, 1413.
14 H. Schmidle, S. Jäger, C. K. Hall, O. D. Velev and S. H. Klapp, *Soft Matter*, 2013, **9**, 2518.
15 R. M. Erb, H. S. Son, B. Samanta, V. M. Rotello and B. B. Yellen, *Nature*, 2009, **457**, 999.
16 K. H. Li and B. B. Yellen, *Appl. Phys. Lett.*, 2010, **97**, 083105.
17 B. B. Yellen, O. Hovorka and G. Friedman, *Proc. Natl. Acad. Sci. U. S. A.*, 2005, **102**, 8860.
18 K. Aoki, K. Furusawa and T. Tanaka, *Appl. Phys. Lett.*, 2012, **100**, 181106.
19 J. Faraudo, J. S. Andreu and J. Camacho, *Soft Matter*, 2013, **9**, 6654.
20 W. B. Russel, D. A. Saville and W. R. Schowalter, *Colloidal Dispersion*, Cambridge University Press, 1989.
21 S. Melle, O. G. Galderón, M. A. Rubio and G. G. Fuller, *J. Non-Newtonian Fluid Mech.*, 2002, **102**, 135.
22 J. F. Brady and G. Bossis, *Annu. Rev. Fluid Mech.*, 1988, **20**, 111.
23 D. Frenkel and B. Smit, *Understanding Molecular Simulation: From Algorithms to Applications*, Academic Press, New York, 2nd edn, 2002.
24 T. X. Liu, X. L. Gong, Y. G. Xu, S. H. Xuan and W. Q. Jiang, *Soft Matter*, 2013, **9**, 10069.
25 T. X. Liu, Y. G. Xu, X. L. Gong, H. M. Pang and S. H. Xuan, *AIP Adv.*, 2013, **3**, 082122.
26 D. J. Klingenberg, C. H. Olk, M. A. Golden and J. C. Ulicny, *J. Phys.: Condens. Matter*, 2010, **22**, 324101.
27 D. J. Klingenberg and J. C. Ulicny, *Int. J. Mod. Phys. B*, 2011, **25**, 911.

